

EBSD ANALYSIS OF PHASE COMPOSITIONS OF TRIP STEEL ON VARIOUS STRAIN LEVELS

Ondřej Man^{1*}, Libor Pantělejev¹, Zbyněk Pešina¹

Received 16th April 2009; accepted in revised form 5th May 2009

Abstract

Flat test bar made of TRIP steel was sequentially strained in tension. Each deformation step was made on a predefined strain level in which the phase composition was measured using EBSD; the analyses were made ex-situ exactly in the same area of 30x30 μ m. Retained austenite (RA) was present in the form of elongated grains (plates) and roughly equiaxial ones. The RA content was initially 14.5% and decreased with imposed strain down to approximately 5% in selected strain range from 0% to 10%. This is in agreement to some extent with outcomes of both in-situ and ex-situ experiments presented by other authors, the difference being supposed either in data clean up or in variation in microstructure of particular steel. Kernel average misorientation method was confirmed as useful tool to discern bainite and grainy ferrite in lightly deformed specimen. Problem arose in distinguishing between martensite and deformed ferrite at higher deformation levels because of high dislocation density and/or lattice distortion in both components. The ferrite and retained austenite fraction were analysed with sufficient accuracy; martensite fraction was established with high degree of uncertainty.

Keywords: Electron backscattering diffraction (EBSD); TRIP effect; Retained austenite.

1. Introduction

One group of engineering materials that attracts interest for a period of time already is the set of TRIP assisted steels because of their promising mix of strength and plasticity [1].

The key issue in understanding the TRIP effect (Transformation Induced Plasticity) is to clearly distinguish the phases present in the microstructure and their transformations in the course of plastic deformation. In order to achieve this, there are several methods available: (a) X-ray and neutron diffraction, magnetic measurement, (b) suitable etching route and light optical microscopy and (c) scanning electron microscope (SEM) based techniques such as electron backscattering diffraction (EBSD). General features of these techniques are: ad (a) - provide accurate averaged information from large area or volume of a sample but no locally specific data; ad (b) - are not always sufficiently distinctive because e. g. colour etching does not render each structure component uniquely but are fast on the other hand; ad (c) - needs careful specimen preparation and often time

consuming SEM operation but can provide sufficiently detailed information on the phase distribution inside the analysed area [2, 3].

For the present work, the EBSD method was chosen as a basic tool to identify phases and their mutual relations; the reason was firstly the ability to keep track of the phases in the selected area of interest during straining and secondly reasonable accuracy of the method. Although this particularly applies in case of in-situ experiments the same goal is likely to be achieved by the ex-situ procedure we employed.

Many authors have done EBSD aided analyses of phase composition of TRIP steel (see [3-8]). They focused either on retained austenite (RA) content and its development under imposed strain [7, 9], omitting to discern between bainite, ferrite and martensite, or to proper phase identification without imposing any strain [2, 4-6] or just comparing undeformed and slightly deformed specimens [3, 8]. Across all these studies, orientation relationships between parent austenite and product ferrite are mentioned as well as textures of both phases and its evolution with straining.

¹ O. Man, Ing.; L. Pantělejev, Ing. Ph.D., Zbyněk Pešina, Ing. – Institute of Materials Science and Engineering, Faculty of Mechanical Engineering, Brno Technical University, Technická 2, 616 69 Brno, Czech Republic.

*Corresponding author, e-mail address: man@fme.vutbr.cz

Concerning the methodology of the phase differentiation, there can be seen two different approaches: first - relying purely on the indexing capability of the acquisition software to discern between FCC and BCC structure without further data processing (e. g. [5]) and second - using the “as indexed” FCC/BCC classified data set as a raw material for further analysis (e. g. [2-4, 6-8]).

The latter approach is again applied in various ways. Petrov et al. [3, 8] used mainly the image quality (IQ) and confidence index (CI) parameter to differentiate between bainitic and grainy ferrite. Zaefferer and coworkers [2, 6] preferentially adopted another parameter, the kernel average misorientation angle (KAM). The idea in the background of both these approaches is the same: grainy ferrite undergoes recrystallization to some extent during the low temperature isothermal treatment and therefore exhibits low dislocation density [3, 8]. Bainitic ferrite grows during the cooling from intercritical annealing point and the low temperature isothermal treatment. It exhibits markedly increased dislocation density which manifests itself in varying level of both parameters discussed due to their sensitivity to the density of lattice defects.

The IQ and CI parameters are measures of EBSD pattern quality which is coupled to dislocation density, provided all other factors are negligible or constant (specimen preparation route, surface relief). The KAM parameter is on the other hand a measure of lattice distortion – it provides average misorientation between the kernel (data point) and its close neighbours or the next ones or even the next-next ones; the order of neighbours serves to control the length range in which the orientation comparison is done. KAM value depends mainly on the EBSD grid pitch and SEM resolution and is pretty immune to external factors like those spoken in case of IQ and CI parameters. It seems that the KAM evaluation method is the best for distinguishing the bainitic and grainy ferrite.

Detailed study of Zaefferer [6] evidenced the extent of specific orientation relationships between the parent austenite and herefrom growing ferrite by comparison of the EBSD data with TEM measurements: the boundary between the RA grain or laths and bainitic ferrite laths is closely arranged according to Kurdjumov – Sachs orientation relationship (KS-OR) and the boundary between massive RA grain and proeutectoid ferrite pursues this OR with some tolerance. In fact, there are actually two ORs likely to be observed: the KS-OR and the Nishiyama – Wasserman OR (NW-OR) but these

orientation relationships often coincide while measured by EBSD due to little angular difference between them. Another possible ORs are the Bain’s and by Pitsch but non of them are observed in larger scale in practise [4]. These specific ORs can be utilized to verify the position of RA – ferrite interface.

In this work we focused on testing the KAM evaluation method for phase composition assessment of a given TRIP steel in undeformed state and its comparison with neutron diffraction data. Since this method was not yet applied to the natural as strained and therefore “embossed” specimen surface, we further tested the ability of this method to discriminate the bainitic and grainy ferrite in a 30 μm x 30 μm area of interest on a single gradually strained specimen. The IQ and CI method after Petrov was rejected due to its sensitivity to surface relief which is expected to develop.

2. Experiment

2.1. Material

The material for this study was Si added TRIP steel, produced by COMTES FHT company, with the composition given in table 1. Its thermomechanical treatment consisted of austenitization of the round steel rod at 1000°C, two consecutive compressive deformations in mutually perpendicular directions, isothermal delay at 750°C, water cooling to 420°C and isothermal delay followed by air cooling. The resulting shape was a flat billet of approximately 14 mm thickness, 30 mm width and 70 mm length.

Tab. 1

Chemical composition of examined steel.

C	Mn	Si	P	S	Cr	Ni	Mo	Al
0.21	1.43	1.90	0.017	0.008	0.06	0.05	0.01	0.036

2.2. Specimen preparation

A set of flat bone-shaped tensile test specimens was machined from the billet. The geometry of the specimens was designed to meet the demands of the testing machine, having the minimum gauge length of 20 mm (gauge cross section 3 mm x 4 mm), while maintain suitable dimensions to be accommodated in the SEM chamber.

We spent one specimen for this work. One of the two planar surfaces of the specimen was mechanically ground and polished and then the surface within the gauge length was polished electrolytically through appropriate mask in a solution

of 5.2% of perchloric acid and 94.8% of acetic acid (by volume). Applied voltage was 60 V, electrolyte temperature was held between 27°C and 28°C.

As orientation markings, two Vickers indents were made on the centerline of the specimen at approximately 0.5 mm distance from each other.

2.3. Straining

Application of strain was done by means of universal testing machine Zwick Z020 equipped with flat jaws. The straining was done interruptedly at room temperature and its course is shown in figure 1. The points of interruption were chosen at 0.85% and 10% of global elongation (measured by extensometer) in order to characterise the yielding region and then the proceeding martensitic transformation of the RA. The straining was cancelled at 22.8% elongation when the stress – strain curve began to drop.

After straining the specimen onto each deformation level it was withdrawn from the machine jaws and underwent EBSD analysis. After that it was put back and strained onto another level. The experiment was arranged so as to minimize delay between each loading step and EBSD analysis.

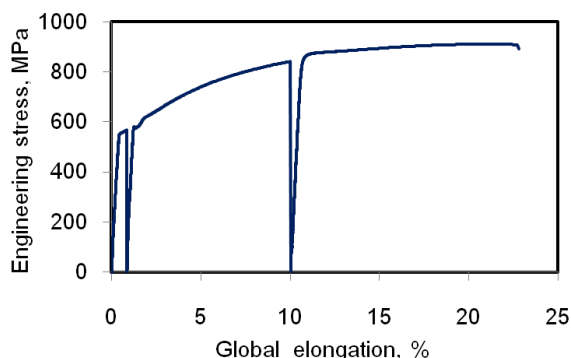


Fig. 1. Combined stress-strain curves of the loading steps

2.4. EBSD

EBSD analysis was done at the initial undeformed state of the specimen and then after each loading step. The area of analysis was 30 μm x 30 μm and was scanned with the step size 0.2 μm in a hexagonal grid. EBSD patterns were recorded at a rate of 2.1 – 3.1 frames per second with 4 x 4 pixel binning by means of DigiView 1612 CCD camera with OIM™ DC 3.5 acquisition software made by TSL. The working distance was set to 12 mm and accelerating voltage to 25 kV. The specimen slope in the Philips XL30 W-filament SEM chamber was 75°. The patterns were automatically indexed based on the minimum of 9 detected bands while 13 bands were set

as maximum. The family of permissible phases was reduced to ferrite (BCC) and austenite (FCC); their crystallographic data were drawn from TSL database.

The data were further processed in OIM™ Analysis 3.08 software. Two step clean up procedure was applied to the orientation data after their acquisition: firstly, the “neighbour phase correlation” algorithm was applied in order to minimize indexing errors by setting the threshold CI value of data points to be affected to 0.06. Secondly the “grain dilation” was applied to clean up the rest of supposedly misindexed points – the grain dilation ablated the single-pixel islands.

2.5. Neutron diffraction

The neutron diffraction measurement were performed on the remaining set of three specimens from the same billet. The RA content was measured at undeformed state only for the reason of time.

Measurements were done at the Institute of Nuclear Research in Řež.

3. Results and discussion

3.1. Mechanical behaviour

The resulting stress – strain curve composed of three segments belonging to each loading step is shown in fig. 1. It should be noted that the deformation throughout the whole range of elongation was purely homogeneous. This conforms to the desired TRIP steel behaviour.

3.2. Retained austenite analysis

After the data clean up a comparison between the RA content resulting from the raw FCC structure data and from the corrected ones was made. This comparison is presented as a dependence on the global elongation in figure 2 together with RA data of similar TRIP steel grades drawn from the literature. It can be seen that our raw data meet closely those presented by Park et al. [9] but no other. This fact can be explained by supposing that Park did not perform any data refinement, although this step is not mentioned in his paper.

The RA data after filtration lie in between the curves representing the RA content evolution after Park et al. and after Petrov et al. [3, 8]. Since Petrov reported the data clean up, it seems that these differences are caused either by the data refinement or by the difference in morphology of RA islands. Park reports both granular and needle (lath) type, Petrov,

on the other hand, shows only granular type RA. The situation is further complicated by the fact that the austenite stabilizing element somewhat differs among the steel grades – some are Si-added and others are alloyed with Al. However, when we take into consideration the Si-type steels only, the spoken difference diminishes but still persists.

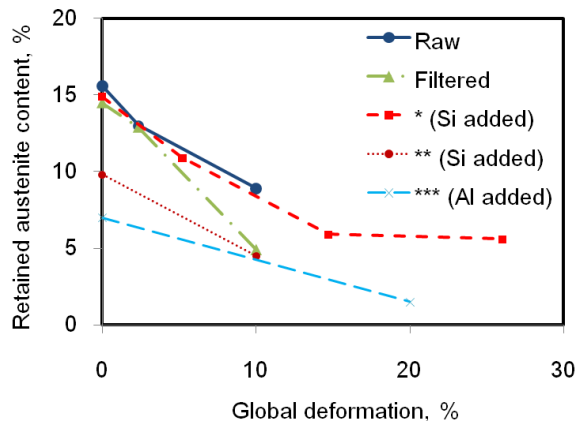


Fig. 2. Dependence of RA content on imposed strain. Combined raw and filtration-corrected data.

Literature data sources: * - [9]; ** - [3]; *** - [8].

The microstructure of the steel under examination contains both RA types as shown in fig. 3. The difference of RA vs. elongation trends between our raw data and the refined ones, together with their relation to data after Park and Petrov seems to indicate combined influence of both factors. This explanation is deemed valid even when we take into account the role of the scanned area size, because these are similar in all papers cited above.

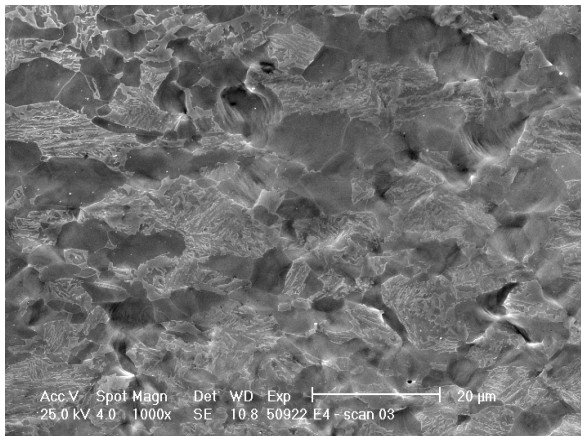


Fig. 3. Deformation 10%. SEM image of the microstructure. Electrolytically polished.

The RA content measured by means of neutron diffraction was established as $10.8 \pm 2.4\%$. This value is comparable to 14.5% measured by EBSD, especially when we take into account that the EBSD

value represents only $30 \mu\text{m} \times 30 \mu\text{m}$ area of the surface.

3.3. Analysis of BCC fraction

KAM evaluation method was employed in order to distinguish between bainitic and grainy ferrite. Maximum misorientation angles up to 5° were tested (i. e. the angles that make the upper limit to the KAM computation – KAMs above this value are omitted). In accordance with Zaefferer [2], the 3° limit was found as the most suitable for the chosen “second neighbour” KAM computation method – see sketch in figure 4. This value defines the largest lattice distortion of $7.5^\circ \mu\text{m}^{-1}$ and the kernel diameter $0.8 \mu\text{m}$.

The KAM data are presented in a graph in figure 4 where the number fractions of particular phase in 2.35% and 10% deformed state are corrected for the RA content decrease. It is obvious from the graph that the KAM profiles for 0% and 2.35% deformation are similar but the profile for 10% deformation exhibits shift of the peaks in KAM distributions towards higher misorientations.

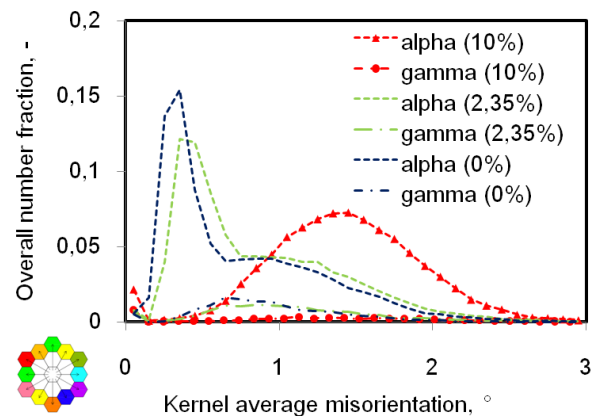


Fig. 4. Kernel average misorientation (KAM) distributions for BCC and FCC partition after 0 %, 2.35 % and 10 % deformation. Sketch in the lower left corner shows a scheme of applied kernel

The peak KAM fraction for austenite moves from 0.65° towards 1.15° with increased deformation. This evidences the increasing curvature of the RA lattice during straining. An exception takes place at near-zero KAM values for 10% deformation, which can be attributed to the decrease of the average RA grain size compared with the kernel size - see table 2. Small grains with diameter approximately equal to the kernel diameter are supposed to have insufficient volume to give rise to large lattice distortions.

Similar trend is observed in KAM profiles for BCC data for 2.35% and 10% deformation. Here the originally bimodal distribution changes into unimodal one with approximately the same modus as the respective KAM profile for austenite. In case of the curve for 10% deformation the same feature near zero misorientations is present. This feature cannot be explained by the kernel and grain diameter coincidence this time. The most probable explanation is the increased number of incorrectly indexed points due to imposed plastic deformation and surface relief.

Tab. 2

Average grain size of BCC and FCC phases by area fraction. Grain boundary defined where the point-to-point misorientation exceeds 5° .

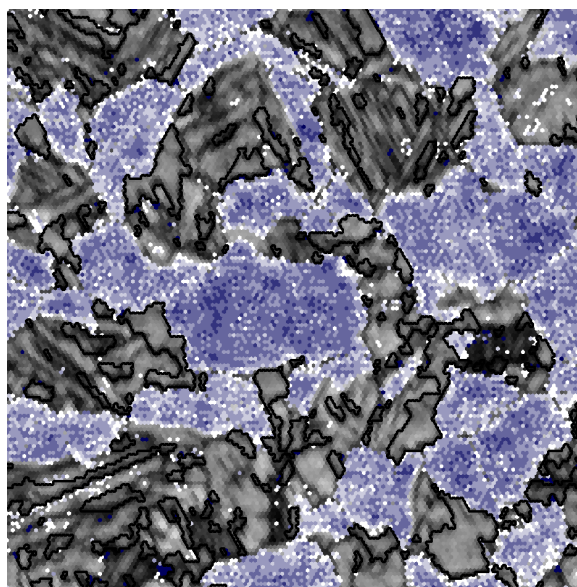
Phase	Average grain diameter [μm]		
	Elongation [%]		
	0	2.35	10
FCC	1.68	1.29	0.94
BCC	4.72	4.19	4.76

The KAM profiles for BCC data partition were used to find the threshold value which could provide the division line between bainitic ferrite and the remnant grainy one. The threshold was sought by visual comparison of the location and extent of the area with KAM value above and below tested value. This procedure resulted in the threshold value 0.6° , which is also valid for the 2.35% deformation profile. The threshold found by such procedure falls between the two apparent moduses in the KAM profile, close to the low misorientation one. It should be noted that more advanced procedure like deconvolution of the peaks in the KAM profile or ferrite grain smoothing algorithm [2] would benefit to the accuracy. An example of the resulting bainitic/grainy ferrite discrimination based on 0.6° KAM value is shown in figure 5 together with respective KAM distribution histogram. The colour coding in the IQ map with phase boundary network agrees with the classes of the histogram that belong to the grainy ferrite region.

In case of 10% deformation, the above described approach is not applicable since the KAM profile is strictly unimodal and therefore does not exhibit any distinguishable peak overlap. The bainitic and grainy ferrite cannot be distinguished by means of KAM evaluation at such degree of deformation.

Moreover, in the deformed state, there is martensite likely to be present. The attempt to use the IQ parameter distribution to resolve the martensite

was also unsuccessful due to similar IQ value of highly deformed ferrite grains and supposed martensite islands. The fraction of martensite was estimated based on an assumption that martensite could have originated only from RA grains, therefore the growing fraction of martensite is on account of the RA content.



7.00 μm = 35 steps IQ 29.983...157.13

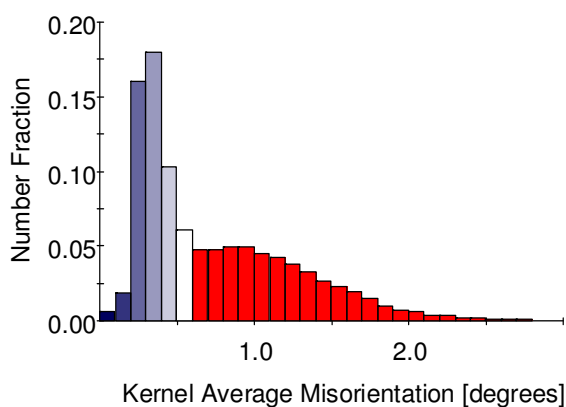


Fig. 5. Deformation 0%. Image quality (IQ) map (upper, grayscale) with phase boundary network (black lines) and areas of BCC phase coloured according to KAM histogram classes below 0.6° threshold (below). Coloured areas are low distortion grainy ferrite

The visualization of this result is given in figure 6, which depicts the development of each structural component fraction in dependence on the global deformation. It can be clearly seen that at 0% deformation the structure is sorted by EBSD into these fractions: 14.5% RA + 49.2% grainy ferrite + 36.3% bainitic ferrite. The sum of the bainitic ferrite and RA fraction gives 50.8% which is in excellent agreement with the supposition that the well balanced microstructure of the TRIP steel during

austenitization should contain approximately 50 to 50% of ferrite and austenite [3].

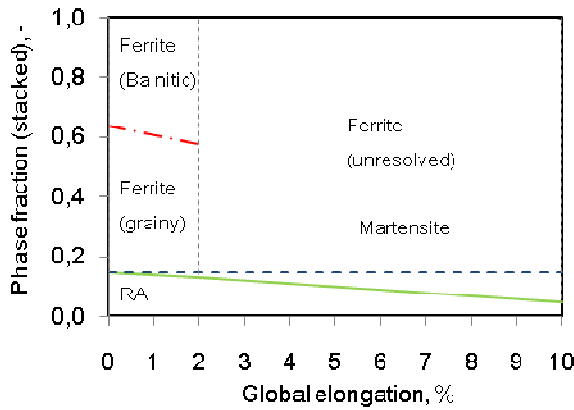


Fig. 6. Stacked diagram of the structure components fraction as a function of imposed strain.

3.4. Orientation relationships

As a secondary tool to identify bainitic ferrite islands we employed the analysis of orientation relationships between austenite and ferrite phase. In order to perform this in a representative manner we calculated the misorientation distribution function (MDF) of the FCC/BCC interface. It gives us clear picture of the occupancy of particular misorientation axis directions as well as occupancy of respective misorientation angles. Figure 7 contains MDF slices for the undeformed state with the most pronounced phase boundary texture components encircled. The solid circle marks the peak that lies approximately at the position of Kurdjumov-Sachs OR expressed as 42.85° rotation about <17.8 17.8 96.8> axis [2], while the dotted one marks approximately the variant of this OR expressed as 90° rotation about <1 1 2> axis [3].

The MDFs of the deformed states exhibit the same appearance, differing only in intensity of the preferred misorientations; the intensity of both main peaks decreases with imposed strain. This trend could be explained by diminishing fraction of RA and therefore decreasing length of BCC/FCC boundaries with specific OR, i. e. the random misorientation background increases. Another factor that would be responsible for cancelling the specific ORs between ferrite and austenite is the increasing amount of lattice distortion introduced into the ferrite areas. Extensively deformed ferrite as well as austenite lattice could cause the phase boundary misorientation to diverge from the ideal KS orientation position. It should be noted that exact differentiation among all possible ORs was almost impossible with current degree of accuracy.

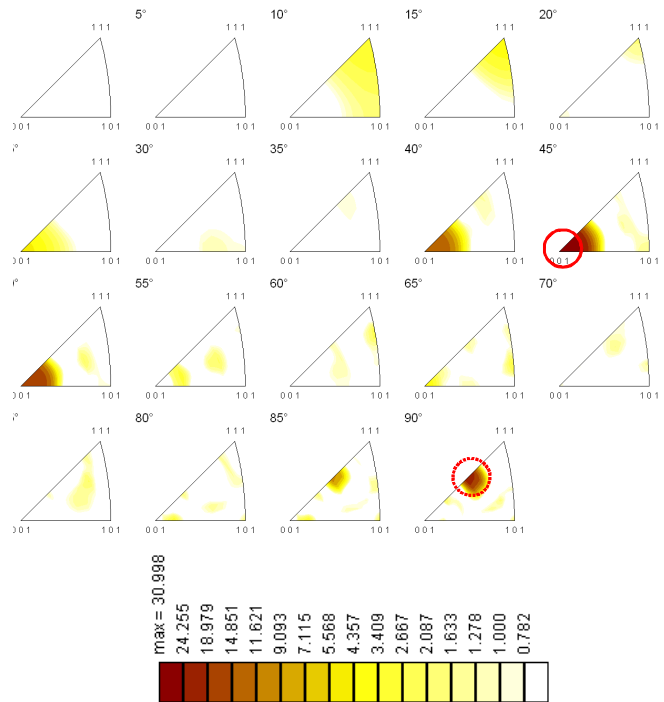


Fig. 7. Deformation 0%. Misorientation distribution function (MDF) of FCC/BCC phase boundaries. Colour key below shows phase boundary texture intensity. Solid and dotted circle mark the most pronounced texture components.

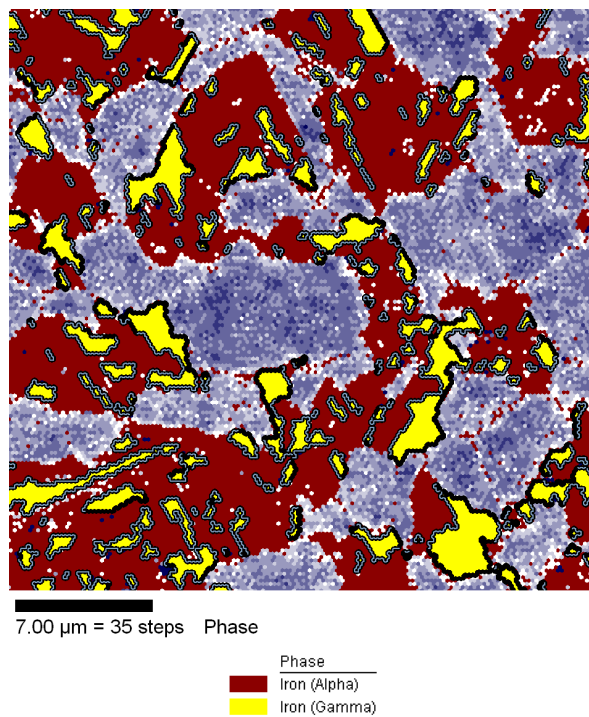


Fig. 8. Deformation 0%. Phase map colour coded according to the key above. Phase boundary network with rather random misorientation outlined by thick black line, thin grey one belongs to the most pronounced MDF peaks with 15° tolerance. Colour gradient overlay has the same meaning as in Fig.5.

The combined FCC and BCC phase map in figure 8 shows the layout of RA islands in undeformed specimen. Another layer of this map is a phase boundary network (in black) with other OR than the most pronounced MDF peaks. Gray boundary network on the other hand depicts the dominant misorientations in the MDF plot. The last information layer is the same as in the figure 5 – the grainy ferrite area shaded according to the KAM value.

By comparison of the coincidence between shaded grainy ferrite and the black outlined random misorientation boundaries it comes out that this correlation is almost regular and vice versa – the remnant bainitic ferrite is related to the RA areas almost solely by the special (KS) orientation relationship within 15° tolerance, which is evidenced by the gray outline of these boundaries.

4. Conclusion

The outcomes of the presented work can be summed up into these conclusions:

- The suitability of the sequential ex-situ experimental procedure for testing the TRIP steel phase composition during straining was verified. We found the surface relief developed under strain as limiting to the accuracy of EBSD analysis. However, the measurement of RA content is not significantly affected by this trade off.
- The KAM evaluation method for distinguishing the bainitic ferrite from the grainy one was tested. It was found that this method is simply applicable on undeformed specimens or just slightly deformed ones; it was confirmed that the method is not appropriate for sample deformation above 2.35 %.
- Based on the KAM evaluation method the phase and structural components of given TRIP steel were identified in the state of 0% and 2.35% deformation. Analysis of the steel deformed to 10% was possible only in terms of FCC and BCC structure discerning.
- The RA content was established as 14.5 % at 0 % strain which decreased to 4.9 % at 10 % strain. The initial division of BCC phase between bainite and grainy ferrite was established to 36.3 % and 49.2 % respectively.
- Special orientation relationships between bainitic ferrite and parent austenite grain were employed to confirm the bainite/grainy ferrite division based on KAM evaluation method.

Acknowledgments

Authors would like to thank Mr. Vadim Davydov with INR Řež for performing the neutron diffraction measurements and prof. Jozef Zrník with COMTES FHT a. s. for providing the experimental material.

References

1. Stejskal, O., et al.: Vliv termomechanického zpracování na vývoj TRIP jevu v Si-Mn oceli, in METAL 2005, 2005, TANGER, s.r.o.: Hradec nad Moravicí.
2. Zaefferer, S., P. Romano, and Friedel, f.: EBSD as a tool to identify and quantify bainite and ferrite in low-alloyed Al-TRIP steels. Journal of Microscopy-Oxford, 2008. 230(3): p. 499-508.
3. Petrov, R., et al.: Microstructure and texture of a lightly deformed TRIP-assisted steel characterized by means of the EBSD technique. Materials Science and Engineering a-Structural Materials Properties Microstructure and Processing, 2007. 447(1-2): p. 285-297.
4. Verbeke, K., Barbe, L. and De Cooman, B.C.: Texture and orientation relationships in phosphorus added TRIP steels. Thermec 2006, Pts 1-5, 2007. 539-543: p. 3347-3352.
5. Wendrock, H., Richter, J. and Guth, A.: The determination of small areas of retained austenite in TRIP-Steels using high resolution electron back scattering diffraction. Praktische Metallographie-Practical Metallography, 2001. 38(6).
6. Zaefferer, S., Ohlert, J. and Bleck, W.: A study of microstructure, transformation mechanisms and correlation between microstructure and mechanical properties of a low alloyed TRIP steel. Acta Materialia, 2004. 52(9): p. 2765-2778.
7. Ryde, L., Hagstrom, J. and Hutchinson, W.B.: An EBSD study of austenite formation and stability in low-alloy TRIP steels. Fundamentals of Deformation and Annealing, 2007. 550: p. 321-326.
8. Petrov, R., Kestens, L. and Houbaert, Y.: Microstructure and microtexture evolution of a TRIP-assisted steel after small deformation studied by EBSD technique. Fundamentals of Deformation and Annealing, 2007. 550: p. 265-270.
9. Park, K.K., et al.: In situ deformation behavior of retained austenite in TRIP steel. Textures of Materials, Pts 1 and 2, 2002. 408-4: p. 571-576.